44th AIAA Aerospace Sciences Meeting and Exhibit
9 - 12 January 2006, Reno, Nevada

AIAA 2006-754

Hydrogen Enriched Confined Methane Flame Behavior and Flashback Modeling

O. Tuncer* and J. H. Uhm†
Department of Mechanical Engineering Louisiana State University, Baton Rouge, LA, 70803

S. Acharya‡
Department of Mechanical Engineering Louisiana State University, Baton Rouge, LA, 70803

Most gas fueled power generation units presently operate on natural gas and many of them would need to tackle the challenges due to a fuel switch towards syngas in the near future. Operating regime of a gas turbine combustor is sensitive to the changes in the fuel composition. Behavior of a premixed enclosed methane-hydrogen flame is studied with regard to thermo-acoustic instability induced flame flashback, emissions, flammability limits and acoustics over a wide range of operating conditions. Hydrogen addition extends the lean flammability limits and enables lower NOx emissions levels to be achieved. However increased RMS pressure fluctuation levels and higher susceptibility to flashback is observed with increasing hydrogen volume fraction. This is associated with higher burning speeds of hydrogen in comparison to methane. Furthermore flashback in the experimental facility is triggered by thermo-acoustic oscillations. Therefore, an analytical model has been developed to capture the flame holding and thermo-acoustically induced flashback dynamics for a pre-mixed gas turbine combustor. A simple linearized acoustic model is derived from the basic conservation laws, and a front-tracking algorithm based on the Markstein's G-equation is coupled to combustor acoustics it in order to track the flame-front which yields in an understanding of dynamic flame holding and flashback behavior. Due to the non-linear nature of the coupling between acoustic velocity and heat release a limit cycle behavior in the flame front movement is observed during simulations. Sets of experiments including phase locked CH radical imaging have been performed in order to time resolve the flame initiation front behavior. Numerical simulations are performed to study flashback and combustor acoustics together and it is found that these are in good qualitative agreement with the experiments.

Nomenclature

A	=	cross sectional area [m^2]
A_f	=	flame area [m^2]
a	=	radius of the center body / fuel exponent [m, -]
B	=	pre-exponential (frequency) factor [$m^3.mol^{-1}.s^{-1}$]
b	=	radius of the annular delivery pipe [m]
b	=	oxidizer exponent [-]
C_A	=	mole fraction of air [-]
C_F	=	mole fraction of methane [-]

* Doctoral Candidate, Department of Mechanical Engineering, 2502 CEBA Bldg. LSU Campus, Baton Rouge, LA, 70803, Student Member AIAA
† Research Associate, TIER Center, 3214G CEBA Bldg. LSU Campus, Baton Rouge, LA, 70803, Member AIAA
‡ L. R. Daniel Professor, Department of Mechanical Engineering, 1419B CEBA Bldg. LSU Campus, Baton Rouge, LA, 70803

Copyright © 2006 by the American Institute of Aeronautics and Astronautics, Inc. All rights reserved.

C_H = mole fraction of hydrogen [-]
c = speed of sound [m/s]
c_d = speed of sound downstream of the flame [m/s]
c_u = speed of sound upstream of the flame [m/s]
c_p = specific heat at constant pressure [$J.kg^{-1}.K^{-1}$]
D = combustor diameter [m]
E = energy of the mode shape [-]
E_a = activation energy [J/mol]
f = flame front function [m]
H = step height at the dump plane [m]
K_f = overall forward reaction rate [$mol.m^{-3}.s^{-1}$]
k = wave number [m^{-1}]
L = combustor length [m]
L_f = flame height [m]
n = temperature exponent [-]
$\hat{n}$ = normal vector [-]
P = pressure [Pa]
q = rate of heat release [Watt]
R = gas constant, radius of the combustor [$J.kg^{-1}.K^{-1}$,m]
R_u = universal gas constant [$J.K^{-1}.mol^{-1}$]
S_L = laminar flame speed [m/s]
Sw = swirl number [-]
s = laplace operator [-]
T = temperature [K]
T_{ad} = adiabatic flame temperature [K]
T_{in} = inlet temperature [K]
t = time [s]
u = longitudinal velocity [m/s]
x = longitudinal coordinate measured from the bottom end of the combustor [m]
x_f = axial position of concentrated heat release [m]
z = longitudinal coordinate measured from the dump plane [m]
r = axial flame coordinate [m]
Δt = time delay [s]
Δx = distance between flashback sensors / grid spacing [m]
ϕ = equivalence ratio [-]
ω = angular frequency [rad/s]
α = thermal diffusivity of the un-burnt reactants / filter coefficient [m^2/s, -]
β = zel'dovich parameter / filter gain [- ,-]
γ = specific heat ratio [-]
δ = delta function [-]
ρ = density [kg/m^3]
ρ_d = density downstream of the flame [kg/m^3]
ρ_u = density upstream of the flame [kg/m^3]
ψ = mode shape [-]
η = amplitude function [-]
G = combustion progress variable [-]
λ = wavelength [m]

I. Introduction

GAS turbine engines are commonly utilized in electricity generation[1]. These modern premixed gas turbine combustors are usually operated very close to the lean blowout limit due to emissions considerations[1]. Lean combustion reduces the adiabatic flame temperature thus reducing the production rate of nitric oxides which is a highly temperature dependent process[2,3]. Yet, as the adiabatic flame temperature is lower carbon monoxide emissions tend to increase. An optimum operating point needs to be sought to guarantee both low nitric oxide and

carbon monoxide emissions. In this operating range flame holding and thermo-acoustic instability become the two most important considerations. Thermo-acoustic instability not only deteriorates the material structure of the combustor wall subjecting it to fatigue loading[4], but also can induce hazardous flame flashback into the premixing section[5]. From this point of view near lean blowout behavior of synthesis gas needs to be explored in a detailed fashion.

Thermo-acoustic oscillations (also referred as humming or chugging) occur because unsteady heating generates sound waves that produce velocity and pressure perturbations. Inside a combustor these oscillations again couple with the heat release[4]. If the unsteady heat input is in phase with pressure perturbations acoustic waves gain energy and instability becomes possible. In his pioneering work Lord Rayleigh[6] gives a clear physical description of this self-excitation phenomenon. In his own narrative he suggests that

"If heat be communicated to, and abstracted from, a mass of air vibrating (for example) in a cylinder bounded by a piston, the effect produced will depend on the phase of the vibration at which the transfer of heat takes place. If heat be given to the air at the moment of greatest condensation, or be taken from it at the moment of greatest rarefaction, the vibration is encouraged. On the other hand, if heat be given at the moment of greatest rarefaction, or abstracted at the moment of greatest condensation, the vibration is discouraged."

In reality, strength of these oscillations are limited by non-linear effects such as flame hydrodynamics and limit cycle oscillations occur. However, these oscillations can be so strong that they can even cause gas turbine to shut down in order to avoid catastrophic damage. Prolonged exposure to pressure fluctuations shall reduce the lifetime of gas turbine hardware. Thermo-acoustic oscillations also have an effect on flame stability and flame holding. During these oscillations flame boundary also moves[7] as well. The location of the flame-front also affects stability[8]. If adequate conditions are present flame might enter inside the premixing section triggering flashback. This phenomenon is called as thermo-acoustic instability induced flame flashback. For the study of thermo-acoustic instability often the flame is assumed to anchor at a specific point inside the combustor. This assumption is likely to be satisfied in well-stabilized flames, however this paper deals with resolving ill behavior due to poor flame stability. Letting the flame interface move is the only way to study such behavior. On the other hand this approach lacks the fidelity of resolving flame front movement and capturing erratic behavior such as flashback or poor flame holding due to self-excited oscillations.

Synthesis gas (syngas), an environmentally clean source of energy, is a variable mixture of primarily hydrogen (H_2) and carbon monoxide (CO). Energy contribution of syngas in the existing integrated cycle (IGCC) land power generation installations is about 10-20% of the total power output. Depending on the gasification process variables and which solid is gasified (coal or biomass) substantial change in the resulting syngas composition can occur[9]. This change in the syngas composition significantly alters the flame behavior[10]. The quality and composition of the fuel impacts the turbine life and emissions[11]. Therefore characterization flame behavior at different syngas compositions is an extremely important task. In addition, syngas combustion in particular generates many of the adequate conditions for flashback due to high flame speeds associated with its hydrogen content. Moreover, syngas is a low BTU fuel with less chemical bonding energy per unit weight. Therefore, in order to achieve a desired power output from syngas high mass

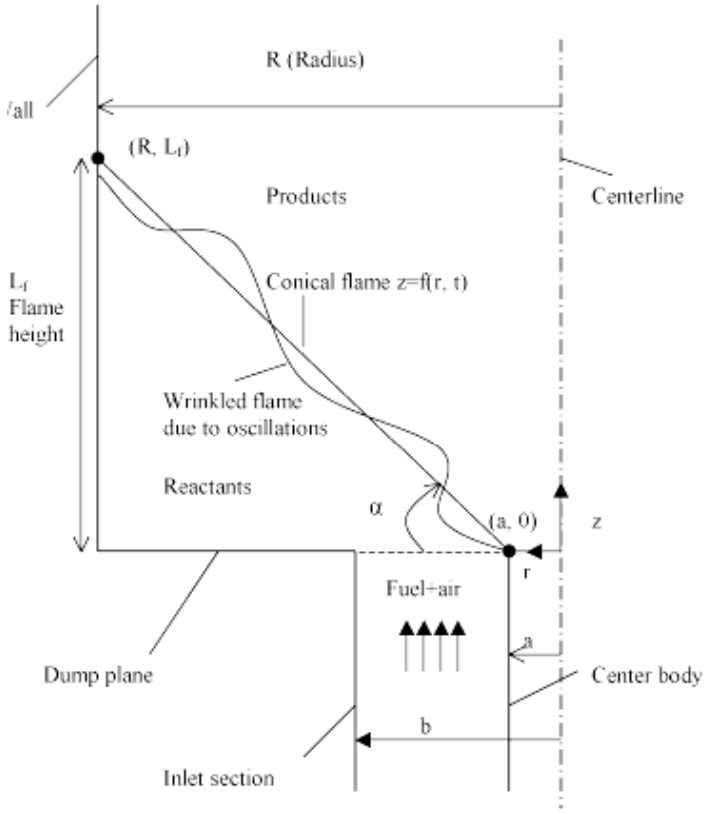

Figure 1. Geometry of the Flame.

flow rates need to be used. High mass flow rates normally translate into higher injection speeds, which pose a significant problem in terms of flame holding[12, 10, 13, 14].The goal of this paper is to develop a simplified mathematical model for flame holding and thermo-acoustic instability induced type flame flashback and to verify it against experimental data. Obviously this type of flashback is not the only one that occurs in combustors. Other flashback types include boundary layer propagation, flashback due to low flow speeds and combustion induced vortex breakdown (CVIB) type flashback. However, boundary layer propagation only occurs at very low speeds, which is not relevant to practical applications. Model developed in this paper can resolve flashback due to low axial speeds but still avoiding this type of flashback is rather trivial and gas turbine combustors are already designed to have sufficient flow speeds inside the pre-mixer. CVIB type flashback occurs due to a mismatch of time scales (chemical and hydrodynamic). In this scenario breakdown of primary re-circulation vortex occurs due to fast heat release and resultantly static pressure builds up inside the combustor forcing the flame into the delivery section. To resolve this phenomenon, flame-vortex interactions should be resolved using an appropriate chemistry and turbulence model. A one-dimensional model would not be sufficient for this task. This type of flashback usually occurs near stochiometric flow conditions. An experimental test facility whose details are discussed in a latter section has been built to study flame holding and flashback characteristics and test model results.

II. Mathematical Modeling

Assuming a quasi one-dimensional flame in a variable area duct the following linearized acoustic model has been obtained from the Euler equations, conservation of energy and equation of state. Details of derivation are left to the appendix section. Interested reader is referred to that section for a step-by-step derivation procedure. However the main underlying assumptions can be summarized as follows; Inviscid flow, one-dimensional flow in a variable area duct, calorifically perfect gas, fully premixed and finally negligible pressure losses along the length of the combustor. These assumptions lead to the following acoustic equations (see Eq. 1 & 2). These equations govern the dynamics of one dimensional acoustic wave motion inside the combustor tube. Near the flame acoustic field in a real combustor is indeed two-dimensional but this two-dimensionality of the field has almost no impact on flame behavior[15].

While solving these equations, fully non-reflecting (closed) and fully reflecting (open) boundary conditions are used for closed inlet and open outlet respectively. The boundary condition imposed by the closed end of the tube is that air particles at the closed end cannot move back and forth since they are adjacent to a wall; they can only be compressed against the end of the tube. Thus pressure can fluctuate maximally at the closed end of an acoustic tube, but particle velocity is zero. Conversely, boundary condition imposed at an open end of an acoustic tube is that air pressure must be equal to ambient air pressure. Air particles at the open end will respond to a pressure wave coming out of the tube not by compressing, since there is no wall to compress against. Thus at the open end of an acoustic tube, a standing wave has maximum fluctuation in volume velocity, but zero variation in air pressure. These boundary conditions (Eqs. 3-4) represent the situation inside the combustor tube realistically.

$$\frac{\partial u'}{\partial t} = -\frac{1}{\rho}\frac{\partial P'}{\partial x} \tag{1}$$

$$\frac{1}{\rho c^2}\frac{\partial P'}{\partial t} + \frac{1}{A(x)}\frac{\partial u' A(x)}{\partial x} = \frac{\gamma - 1}{\rho c^2}\dot{q}' \tag{2}$$

$$u'(x,t)\big|_{x=0} = 0 \tag{3}$$

$$P'(x,t)\big|_{x=L} = 0 \tag{4}$$

In general for a fully premixed flame, combustion occurs within a thin interface that separates fresh and burnt gases. For a one-dimensional situation as in here flame front can be modeled as an infinitely thin plane. This assumption is satisfied on the condition that the axial extent of heat release (diameter of the combustor) is much smaller $D << c/\omega$ in comparison with the acoustic wavelength[4]. Furthermore, in practice combustor is usually a small part of a much large inlet outlet ducting system such that this assumption is justified. Now by concentrating all heat release at the flame base (see Figure 1), such that $x_f(t) = f(a,t)$, Eq. 2 can then be written as follows;

$$\frac{1}{\rho c^2}\frac{\partial P'}{\partial t}+\frac{1}{A(x)}\frac{\partial u'A(x)}{\partial x}=\frac{\gamma-1}{\rho c^2}\left(\dot{q}'\delta\left(x-x_f\right)\right) \tag{5}$$

This approach greatly simplifies the analysis, as one does no longer has to deal with a distributed heat source along the length of the combustor.

Further assuming constant properties before and after the axial location of concentrated heat release;

$$\rho(x)=\begin{cases}\rho_u & x\le x_f\\ \rho_d & x>x_f\end{cases}$$

$$c(x)=\begin{cases}c_u & x\le x_f\\ c_d & x>x_f\end{cases} \tag{6}$$

$$T(x)=\begin{cases}T_{in} & x\le x_f\\ T_{ad} & x>x_f\end{cases}$$

Density, speed of sound and temperature are constant in either side of the flame. Flame front represents a discontinuity over which a sudden jump occurs in these properties. Considering the nature of premixed flames this assumption is a valid one and is often used to simplify the analysis.

System of equations need to be solved are partial differential equation that require both initial and boundary conditions. Further simplification is possible through operating on Equation 5 by $\partial/\partial t$ and on Equation 1 by $\partial/\partial x$ and combining them together such that the acoustic velocity terms drop from the resulting expression.

$$\frac{\partial^2 P}{\partial t^2}+c^2\frac{\partial^2 P}{\partial x^2}=(\gamma-1)\frac{\partial q'}{\partial t} \tag{7}$$

Now using separation of variables technique to express pressure as the product of a time dependent amplitude function η(t) and spatial mode shape function ψ(x), which satisfies the boundary conditions the PDE, can be simplified into an ODE. In fact there exist more than one admissible mode shape yet one can assume a single dominant mode is present without any loss of generality.

$$P'(x,t)=\overline{P}\,\eta(t)\psi(x) \tag{8}$$

Similarly the acoustic velocity u' can be expressed as follows,

$$u'(x,t)=\dot{\eta}(t)\frac{\partial\psi(x)}{\partial x}k^{-2} \tag{9}$$

Plugging Eqs. 8-9 into Equation 7 one arrives at the following ODE (Eq. 10). This is the oscillator equation that governs the acoustic behavior of the combustor.

$$\ddot{\eta}+\omega^2\eta=\frac{(\gamma-1)}{\overline{P}}E^{-1}\psi(x_f)\frac{dq'}{dt} \tag{10}$$

The energy E of the mode shape ψ that appears in Eq. 10 is given by Eq. 11 as follows.

$$E=\int_0^L\psi^2(x)dx \tag{11}$$

Applying the boundary conditions at the inlet and outlet (Eqs.3-4) along with the continuity of pressure condition across the flame interface one arrives at the following acoustic mode shape as in Eq. 12.

$$\psi(x)=\begin{cases}\cos\left(\dfrac{\omega x}{c_u}\right) & x\le x_f\\ \dfrac{\cos(\alpha)}{\sin(\beta)}\sin\left(\dfrac{\varpi(L-x)}{c_d}\right) & x>x_f\end{cases} \tag{12}$$

In the above equation the constants α and β are defined as follows (Eqs.13-14).

$$\alpha = \varpi\, x_f / c_u \tag{13}$$

$$\beta = \varpi \left(L - x_f\right) / c_d \tag{14}$$

Lowest possible frequency of oscillation ω is the smallest root of the following equation. This shall be the dominant acoustic mode of the combustor. Other roots correspond to acoustic modes with higher frequencies. Since only one mode is assumed to be present these need not be solved for.

$$\tan\alpha \tan\beta = \left(\rho_u c_u\right)/\left(\rho_d c_d\right) \tag{15}$$

Should thermo-acoustic instability be predicted with a linear model, without a non-linear one the amplitude and exact frequency of the non-linear limit cycle oscillations would be unpredictable[16]. This is because with a linear model, system response would grow to infinity, an unphysical behavior. Examples of non-linear systems include the response of a violin string to a bow or wind excited oscillations of transmission lines etc. Non-linearity destabilizes the system response until certain amplitude is reached. Beyond this point non-linearity has a stabilizing effect on the system amplitude and reduces the magnitude of the system response. Therefore a limit cycle is established. A stable limit cycle is defined as a closed contour inside the phase plane to which trajectories approach asymptotically. Response of the Van Der Pol equation would be a good mathematical example for this phenomenon.

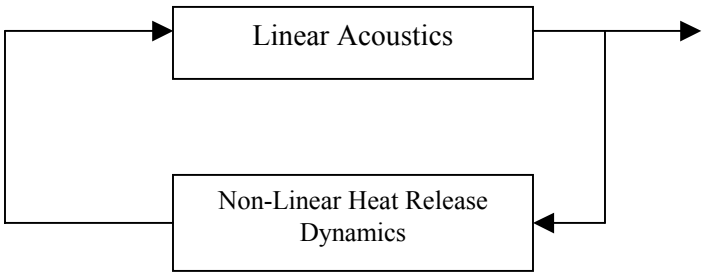

Figure 2. Block Diagram Showing Thermo-Acoustic Coupling.

In the experimental facility a limit cycle behavior is evident from the periodic finite-amplitude up and down movement of the conical flame base, which is well correlated with the acoustic instability cycle. The outcome of the mathematical model should at least resemble this kind of physical response. Consequently a purely linear model shall not be sufficient in terms of resolving flame hydrodynamics. In this thermo-acoustic model it is possible to include a non-linearity of such saturating nature in the feedback term (see Figure 2) that relates acoustic velocity to the heat release. For acoustic velocities under a certain value the system exhibits unstable dynamics. On the contrary beyond this critical value the system exhibits stable dynamics. The very physical argument behind this is that the amount of unsteady heat release should be bounded by the amount of fuel available to be burnt. After all the fuel available at the flame location is consumed the unsteady heat release must in fact vanish.

The non-linearity in the feedback equation (Eq. 16) takes care of the desired non-linearity by gradually saturating the heat release in frequency domain. β is the static gain α is the cut-off frequency of the filter. These filter coefficients are obtained by Park et. al. by linearizing the heat release equation[17]. These parameters are functions of the operating conditions (equivalence ratio, residence time etc.). For small values of fluctuating mass flow rates the system behaves just like a first order linear time invariant filter. However, at larger disturbances the term in parenthesis on the right hand side introduces a non-linearity by saturating the heat release output. Due to this saturation effect a stable limit cycle can be reached. This is consistent with the physical considerations outlined in the preceding paragraph.

$$\dot{q}'(s) = \frac{\beta}{s+\alpha}\dot{m}'(s)\left(1 - \left|\frac{\dot{m}'(s)}{\bar{\dot{m}}}\right|\right) \tag{16}$$

A level set based front tracking method is used to resolve flame front dynamics. Premixed flame stabilizes on the fuel injector tip, which acts like a center-body. Assuming an axisymmetric flow field and further assuming that combustion occurs on a surface whose axial position is given by a single-valued function $z = f(r,t)$, flame surface can be defined by a level-set of the well-known G-equation $G(z,r,t) = 0$. G-equation allows one to decouple dynamics of the reacting flow field from chemistry[18].

$$G(z,r,t) = z - f(r,t) \tag{17}$$

Flame surface G=0 moves towards the side of the un-burnt reactants along its normal direction with a laminar flame speed S_L relative to the oncoming fluid velocity. This phrase can be expressed mathematically as follows (Eq. 6). Note that velocity appearing in these equations is the total flow velocity, which is the sum of mean and instantaneous (acoustic) components.

$$\frac{DG}{Dt} = \frac{\partial G}{\partial t} + \left(\vec{u} - S_L \hat{n}\right).\nabla G = 0 \tag{18}$$

Now plugging in G from Eq. 6 and expressing the normal vector as $\hat{n} = \nabla G / |\nabla G|$ yields in the following equation.

$$-\frac{\partial f}{\partial t} + u - v\frac{\partial f}{\partial r} = S_L \left(1 + \left(\frac{\partial f}{\partial r}\right)^2\right)^{1/2} \tag{19}$$

Neglecting the radial component of velocity as both the mean and fluctuating (acoustic) component of the velocity were assumed to be one dimensional Eq. 7 can be written in a simpler form as,

$$-\frac{\partial f}{\partial t} + u = S_L \left(1 + \left(\frac{\partial f}{\partial r}\right)^2\right)^{1/2} \tag{20}$$

Self-excited oscillations in a ducted can be sufficiently intense $O(\overline{u}) \approx O(u')$, so that flame can leave its attachment point and propagate upstream[19]. For flow velocities less than flame speed (particularly high for hydrogen fuel) flame cannot remain attached at the tip and starts to propagate downstream. Therefore the boundary condition of Eq. 8 at $r = a$ should take this flashback phenomenon into consideration. In addition to de-attachment flame remains perpendicular to the center body to assure zero normal velocity on the wall of the flame-holder on both sides of the flame. Eq. 9 as per[19] prescribes the appropriate boundary conditions for the flame-front equation. Apparently there is a certain hysterisis associated with this boundary condition treatment. Such hysterisis effect however is observed in the Schlieren images of Jones[20].

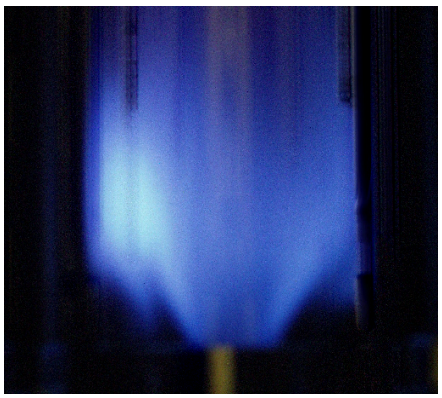

Figure 3. Conical CH_4 Flame Inside the Combustor.

$$\left.\frac{\partial f}{\partial r}\right|_{r=a} = \begin{cases} \dfrac{\left(u^2 - S_L{}^2\right)^{1/2}}{S_L} & if \quad u(t) \geq S_L \wedge \quad f(a,t) = 0 \\ 0 \quad if \quad u \leq S_L \vee \quad f(a,t) < 0 \end{cases} \tag{21}$$

Apparently this approach introduces one more dynamic coupling mechanism into the picture, which is anticipated to be important in the study of poorly stabilized flames, which are prone to blow-off or flashback.

Using Reynolds time averaging concept mean position of the flame front is a conical surface attached at the tip of the center-body (see Figure 3) as it is given in Eq. 22.

$$f(r) = \frac{(r-a)\left(u^2 - S_L{}^2\right)^{1/2}}{S_L} \tag{22}$$

Laminar flame speed appearing in the above equations can be easily obtained from basic theory. Laminar flame speed S_L is expressed in Eq. 23 as a function of Zel'dovich parameter, thermal diffusivity and the reaction rate K_f.

$$S_L = \sqrt{2\beta^{-2}\alpha K_f} \tag{23}$$

where the Zel'dovich parameter β is expressed in Eq. 24 as,

$$\beta = \frac{E_a}{R_u T_{ad}{}^2}\left(T_{ad} - T_{in}\right) \tag{24}$$

And the forward reaction rate is determined using single step generalized chemistry such that,

$$K_f = B.[Fuel]^a [Oxidizer]^b T^n \exp\left(-E_a / RT\right) \tag{25}$$

For a mixture of gases flame is assumed to propagate at a speed associated with the component that has the highest flame speed. For hydrogen enriched methane this component is hydrogen most of the time above a certain hydrogen mass content. Table 1 shows the reaction rate parameters such as temperature exponent n, pre-exponential factor B and activation energy E_a. These parameters are used for the calculation of K_f that appears in the laminar flame speed equation (see Eq. 11).

Reaction	n	a	b	B	E_a (kJ/kmol)
$CH_4 + 2O_2 = CO_2 + 2H_2O$	0	-0.3	1.3	$1.9.10^5$	48.4

Table 1. Reaction Rate Parameters for Methane[2].

Flame area, which affects heat release through Eq., 4 can be calculated by evaluating the following integral.

$$A_f = \int_a^R 2\pi r \sqrt{\left(1 + \left(\frac{\partial f}{\partial r}\right)^2\right)} dr \tag{26}$$

Moreover, a fully implicit scheme is chosen for time integration of acoustic equations due to its unconditional stability. Original flame front level set equation is a type of H-J (Hamilton-Jacobi) equation, which poses certain difficulties during numerical solution as it admits non-smooth solutions, which do not make any physical sense. For this reason flame front equation and the corresponding boundary condition are transformed into an equivalent weakly hyperbolic conservation equation form and discretized on a radial grid with a 5th order WENO (weighted essentially non-oscillatory) scheme. Initial value of the flame front $f(z,0)$ is set to its time averaged conical position as described in Eq. 10 and integrated explicitly using a 3rd order TVD (total variation diminishing) Runge-Kutta method. More detail on numerical solution is provided in the appendix section.

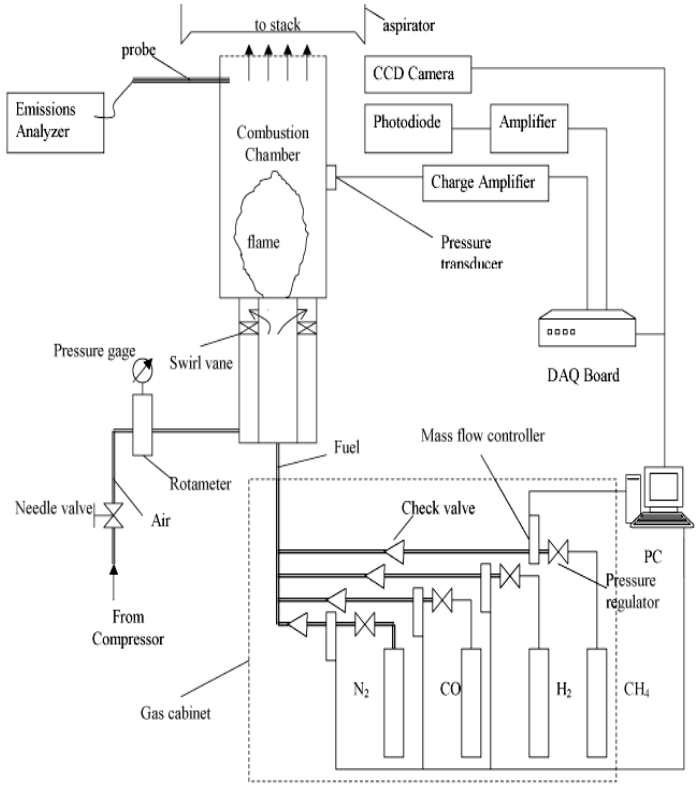

Figure 4. Schematic of the Experimental Setup.

III. Experimental Apparatus

In this section details of the experimental apparatus are discussed. Major components of the experimental setup are depicted in Figure 4. combustor shell, which follows the inlet and premixing sections, is comprised of two pieces. A 3.25" inner diameter quartz tube sits on a 316 stainless steel flange, which defines the dump plane of the combustor. This quartz tube enables optical access to the main re-circulation zone where combustion takes place. This optical access zone enables photodiode, radical imaging, and PLIF measurements. Design of this laboratory scale combustor represents actual premixed combustor designs. Combustor is operated up to a power rating of 20 kW. Quartz tube and the stainless steel shell are cooled by means of forced convection during combustion.

Combustion air is fed through an eight-blade 45º-swirl vane with inner and outer diameters of 19 and 36 mm respectively (see Figure 5). A correlation suggested by Beer and Chigier[21] gives the corresponding swirl number as Sw= 0.98. Swirl not only provides stabilization at the dump plane but also facilitates the entrainment of fuel jets within the cross flow at the pre-mixing zone. The distance between the swirl vane and fuel injection holes are adjusted such that the swirling airflow is fully developed when it reaches the location of fuel injection. This assures good mixing between fuel gas and combustion air within a short downstream distance.

Hydrogen H_2 and methane CH_4 are all individually supplied from compressed gas tanks and mixed inside a manifold before the combustor inlet (see Figure 4). Both their flow rates are monitored by separate mass flow meters. Mass flow rates of carbon monoxide and hydrogen are adjusted separately to achieve the desired syngas composition. Air necessary for combustion is supplied from a 290psig, 450 ACFM Atlas-Copco air compressor. Volumetric airflow rate is measured by a rotameter and a pressure gage at the rotameter exit is used to correct the readings.

Figure 6 shows the variation of cross sectional area along the length of the combustor. Total height of the combustor is 912 mm. The dump plane is located at a non-dimensional length of x/H=0.6. Area expansion ratio at the dump plane is approximately 1:4. At the end of the combustor there is a conical section, which contracts the exhaust flow down to an exit diameter of 12.7 mm.

IV. Results and Discussion

Preliminary measurements are taken using pure methane CH_4, major component of natural gas, in order to establish a baseline for hydrogen enriched methane fuel measurements. Natural gas has been in widespread use for a long time, and it needs to be substituted with other alternate fuels extending fuel flexibility and avoiding its sudden exhaustion. Recently synthesis gas and hydrogen (SGH) fuels appear to be a feasible substitutive solution. However, as mentioned in the introduction section, combustion of SGH fuels has different technological needs since these fuels have much different combustion characteristics from natural gas such as flame behavior and emissions levels.

Table 2 shows an ensemble of flow conditions used during the experiments. Flow

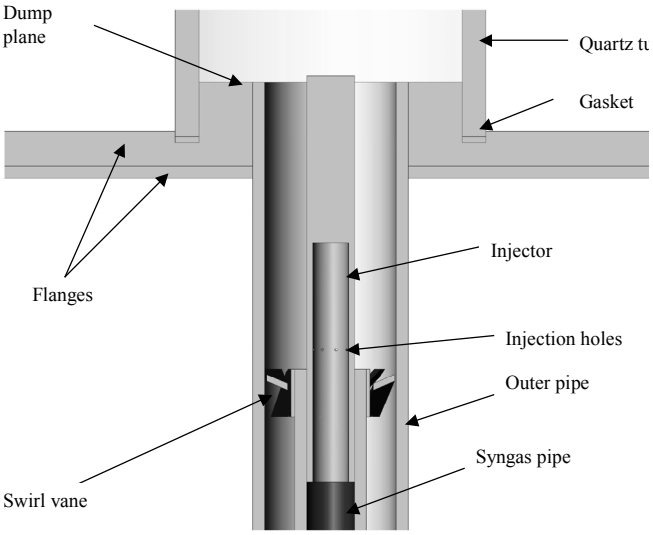

Figure 5. Schematic of the Syngas Delivery Section.

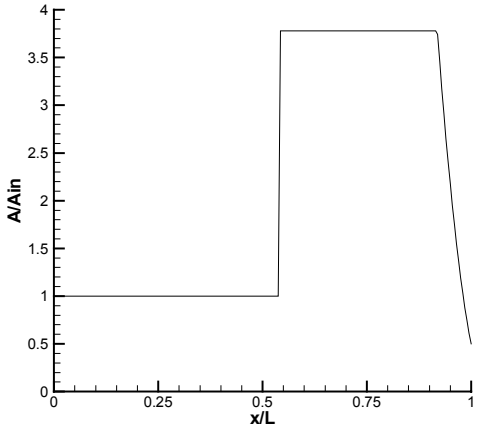

Figure 6. Cross Sectional Area Variation along the Length of the Combustor.

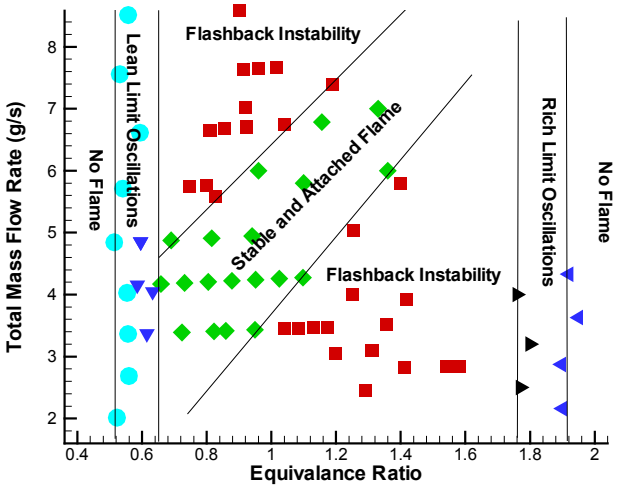

Figure 7. Combustor Operating Regimes (Pure CH_4).

conditions are assigned case numbers for easy referral within the article. During measurements authors have systematically added hydrogen to methane with 10 % increments on a volume basis up to 50 % hydrogen content.

A. Combustor Operating Regimes

First of all it is important to identify different operating regimes of the combustor prior to making detailed studies at desired load conditions. Figure 7 identifies distinct operating regimes as a function of equivalence ratio and total mass flow rates. Each symbol corresponds to a data point and boundaries are drawn on the figure in order to clearly identify the separate regimes. The pre-mixed combustor, exhibits near limit oscillations in the form of cyclic flame extinction and re-ignition within the close vicinity of lean and rich blowout equivalence ratio limits. Such behavior is very typical of gas turbine combustors especially for pre-mixed type ones. In between those two lies a distinct stable regime depicted with diamond shaped symbols where the conical flame tip remains attached at the tip of the center body at all times. On the other hand flashback instability regime marked with rectangles is concentrated at two separate regions in either side of the stable region confined by one of the near limit behavior boundaries. In the event of flashback flame tip leaves the tip of the center body propagates upstream towards the pre-mixing region and re-attaches at the tip again (see Figure 14). This behavior repeats itself in a cyclic manner. Note that this type of ill behavior is encountered at relatively low or high mass flow rates. At low flow mass rates the axial flow velocity is lower which results in a narrower cone angle. Low ratio of u/S_L makes it easier for pressure fluctuations to detach the flame tip. Hence flashback can occur even at moderately low RMS pressure fluctuations. On the other hand flashback instability is also encountered at elevated mass flow rates, which in fact correspond to higher velocities and therefore steeper cone angles for the flame. By referring to the combustor pressure map (see Figure 9) one can see at these operating conditions pressure pulsations are much stronger in the amplitude. More elaborate discussion on the nature of flashback is provided in a latter section of this paper along with some numerical simulation results

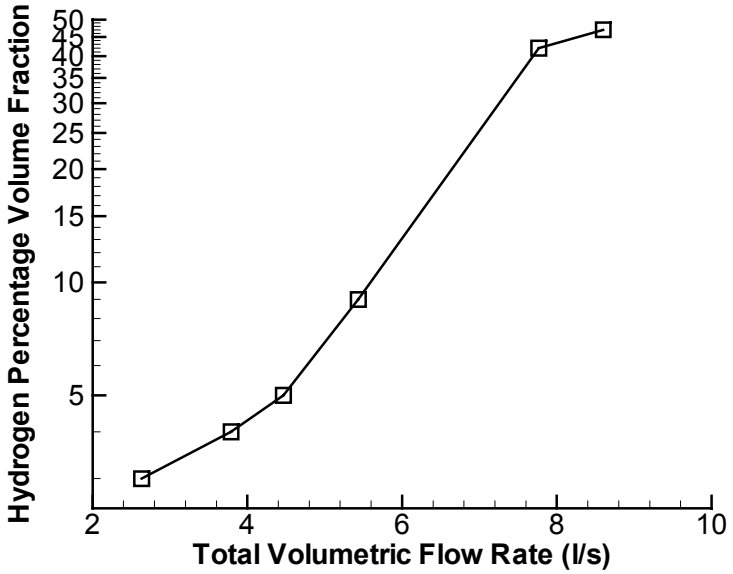

Figure 8. Effect of Volumetric Flow Rate and Hydrogen Fraction on Lean Blowout ϕ=0.55.

Case No	% CH4 in fuel (by volume)	% H2 in fuel (by volume)	Air flow rate (l/min)	Equivalence Ratio
1	100	0	215	0.94
2	50	50	382	0.62
3	100	0	150	1.00
4	70	30	374	0.90
5	60	40	340	0.70

Table 2. Operating Condition Reference Table.

In contrast to natural gas, synthesis gas flame has a much different flow behavior due to both different laminar flame speed and adiabatic flame temperature. Both laminar flame speed and adiabatic flame temperature heavily depend on mixture composition. Since there are multiple fuels in a methane and hydrogen mixture a suitable definition of the equivalence ratio, which takes the overall stoichiometry into account, is needed. Following the assumptions of Yu et. al.[22] an equivalence ratio is defined as follows (see Eq. 27). This equation implies that the

hydrogen in the blend is completely oxidized and the remaining oxygen is used to burn the methane content. This is a reasonable assumption since the hydrogen oxidation proceeds much faster than methane oxidation.

As mentioned in the introduction section contemporary land based gas turbine engines are operated near their lean blow-off limits due to emissions considerations. Here blow-off limits for the laboratory scale combustor are identified with respect to the particular choice of fuel or fuel composition for that matter.

$$\phi = \frac{C_F \Big/ \left[C_A - C_H \Big/ \left(C_H / C_A \right)_{st} \right]}{\left(C_F / C_A \right)_{st}} \tag{27}$$

Hydrogen enrichment considerably extends the lean blowout limits of the methane fuel as evidence to this argument is shown in Figure 8. For a pure methane flame lean blowout is experienced near $\phi \approx 0.7$ yet with hydrogen enrichment flame was sustained at $\phi = 0.55$. As Figure 8 suggests, the higher the volumetric flow rate (hence velocity) the more the amount of hydrogen added to methane in order to keep the reaction going. It is observed that for hydrogen enriched methane lean blowout equivalence ratio is not fixed it both depends on the extent of enrichment and on the flow rate.

B. Heat Release and Pressure Measurements

A number of Kistler 7061 water-cooled piezo-electric pressure transducers are mounted along the combustor wall measures dynamic pressure variations in the combustor. So as to examine the waveform of the combustion instability pressure inside the reactor is to be measured at several stations along the entire length of the combustor.

The CH/OH radical light intensity is recorded using a silicon PIN photodiode (Melles-Griot) looking at the flame equipped with an appropriate band-pass optical filter. Photodiode reading is taken as a measure of integral heat release fluctuations in the main reaction zone of the reactor.

Figure 9 shows the root mean square (RMS) pressure fluctuation amplitude as a function of load condition. Note that most significant pressure fluctuations occur at higher mass flow rates during lean combustion. In practice most of the pre-mixed gas turbine combustors are operated at lean nominal load conditions to eliminate excessive NO_x production (see Figure 17).

Figure 10 shows the power spectrum of heat release and pressure signals. Both exhibit cyclic behavior as governed by the acoustic modes of the combustor. These modes depend on the boundary conditions at the inlet and outlet. In this particular example the dominant frequency is 120 Hz.

RMS pressure amplitude is affected significantly by the fuel composition. Holding the other two parameters

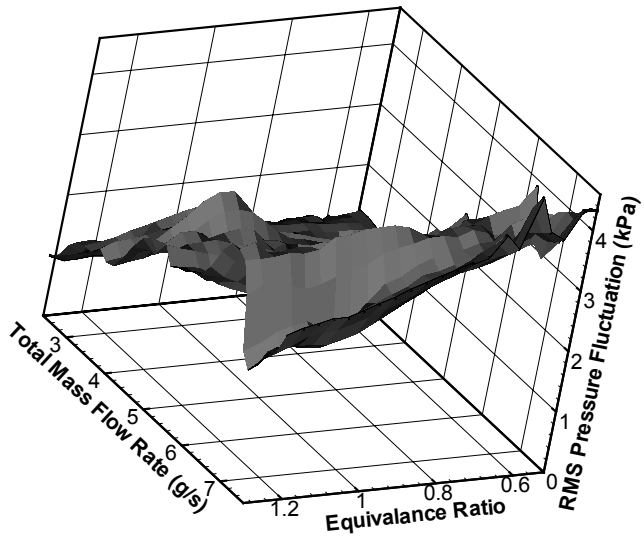

Figure 9. Pressure Map of the Combustor (CH_4 fuel).

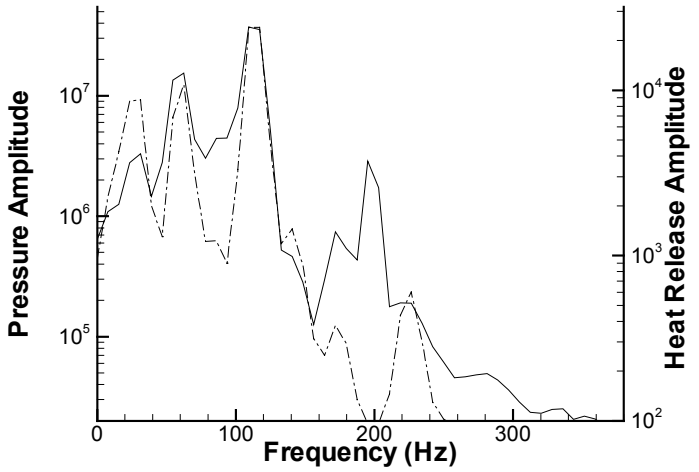

Figure 10. Power Spectra of Pressure and Heat Release Signals (Case 1).

(equivalence ratio and total mass flow rate) constant enrichment of methane with hydrogen yields in higher amplitude pressure fluctuations (see Figure 11). This should be related to the more rigorous oxidation of the hydrogen content of the fuel blend. Higher flame speeds affect flame hydrodynamics defined by the level-set equation. Flame front movement and flashback alters the location of heat release. In the theoretical model this effect is represented via the term $x_f(t)$. Movement of the heat release location can change the instantaneous phase between heat release and pressure fluctuations. This can change the thermo-acoustic instability behavior. Coming back to the figure, depending on the other two parameters that are kept constant an increase in the pressure amplitude as much as 200 % are observed during laboratory experimentation. In addition for pure methane combustion maximum amplitude of 4 kPa is observed.

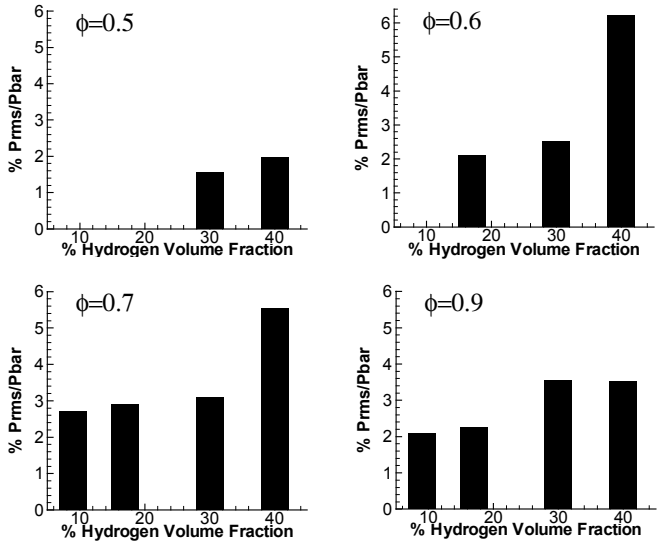

Figure 11. Effect of Hydrogen Volume Fraction on RMS Pressure Levels (Q_{air}=253 lt/min).

C. Flashback Measurements

As mentioned early on another important phenomenon in the study of pre-mixed flames is flame flashback. Flow regimes leading to flashback were identified in Figure 7. Flashback can be triggered by acoustic velocity fluctuations and is much facilitated by higher flame speeds. Different fuels therefore have varying degrees of susceptibility to flashback. This is not only due to a change of flame speed other factors are also present. For example a change in the flame height alters the location of heat release or a change in the flame temperature affects the acoustics by shifting the dominant mode.

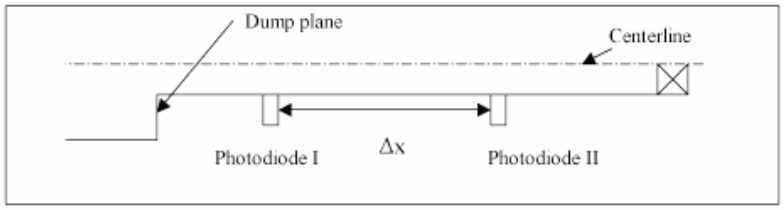

Figure 12. Arrangement for Flashback Speed Detection.

Next figure (see Figure 5) presents evidence that flashback is indeed induced by thermo-acoustic pressure oscillations. The signal on the top is the dynamic pressure history of the combustor whereas the below signal is the voltage reading from the flashback photodiode. At this flow condition (Case 2) pressure trace shows both high and low amplitude fluctuations following one another. When the pressure fluctuations have high amplitude they are strong enough to detach the conical flame from the tip and hence flashback activity is observed as seen in the figure. Once the flame re-attaches (i.e. no flashback activity is observed from the photodiode signal)

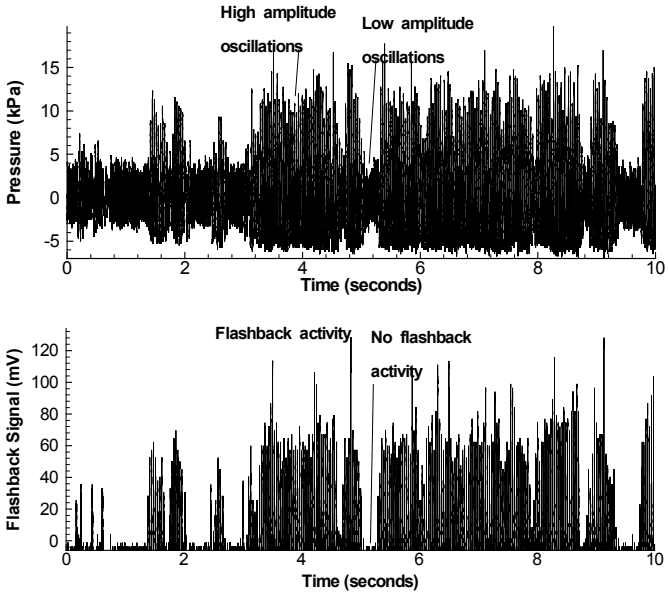

Figure 13. Triggering of Flashback by Thermo-acoustic Instability (Case 2).

pressure amplitude goes down again. Flame front movement and thermo-acoustic phenomena are in fact closely coupled to one another though the dynamic equations presented in this text. Pressure (thus velocity) fluctuations can cause the flame to move. Moreover this flame front movement causes the spatial location of heat release to move thus shifting the instantaneous phase between pressure and heat release while either triggering or killing instability by itself.

A sequence of images is recorded showing the flashback cycle. This cyclic behavior can also be seen in Figure 14 and Figure 16. Initially flame cone makes a steeper angle with the dump plane in order to balance the increase in the oncoming fluid velocity. In the next frame it moves back to its original position and shortly afterwards flame departs from its attachment point and continues to propagate upstream. At one point flame reaches its maximum propagation distance. As the total velocity becomes positive it pushes the flame tip back to its attachment point as seen in the last frame. This behavior is repetitive due to the very nature of velocity fluctuations occurring inside the combustion chamber.

For flashback measurements two sensors separated by a distance of Δx=6.25 mm are utilized (see Figure 12). Photodiode sensors themselves could not be directly mounted on the walls of the delivery section due to space and heating considerations. However light is transmitted to these photodiodes using fiber optic cables. Fiber optic cables had good transmittance and low attenuation within the visible light spectrum.

This specific arrangement not only detects the occurrence of flashback but also enables measurement of its propagation speed. For this purpose the time difference Δt between two flashback signals are recorded and divided by the distance between the photodiodes $\Delta x/\Delta t$. The time delay Δt can be estimated by selecting the peak of the cross-correlation vector between the two-photodiode signals. Later on this propagation speed is compared with laminar flame speed S_L for the same mixture and useful information can be obtained about the nature of flashback phenomenon.

Figure 15 demonstrates the time histories of heat release and flashback signals. Flashback signal is obtained from the fiber optic cable connected to Photodiode I (see Figure 12). This cable is located about 15 mm upstream of the dump plane level where the flame tip stabilizes normally. Therefore a spike in the heat release signal means that the flame has reached that point during

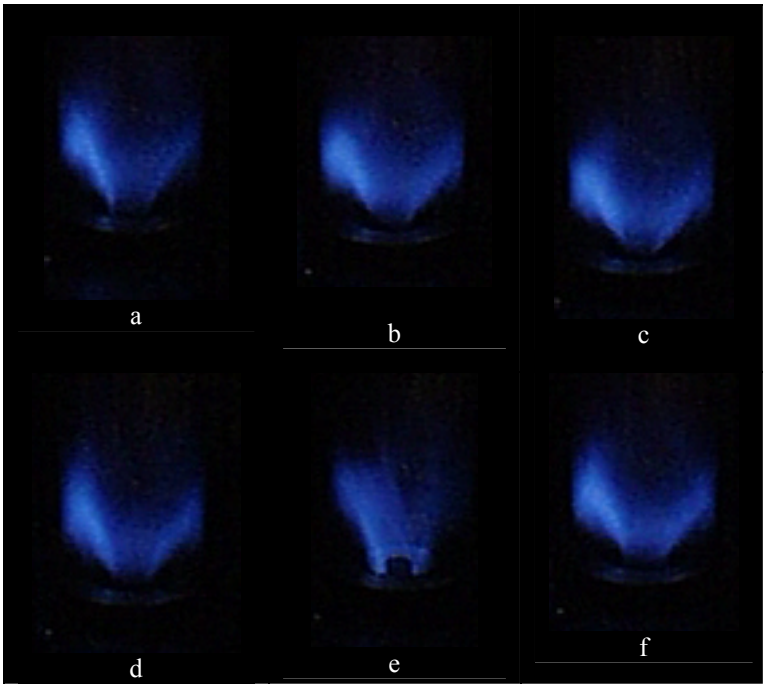

a. Steeper cone angle
b. Moves back to original
c. Departure from the tip
d. Propagation upstream
e. Inside pre-mixing zone
f. Flame re-attaches

Figure 14. Sequence of Flame Images Demonstrating Cyclic Flashback Instability (Case 3).

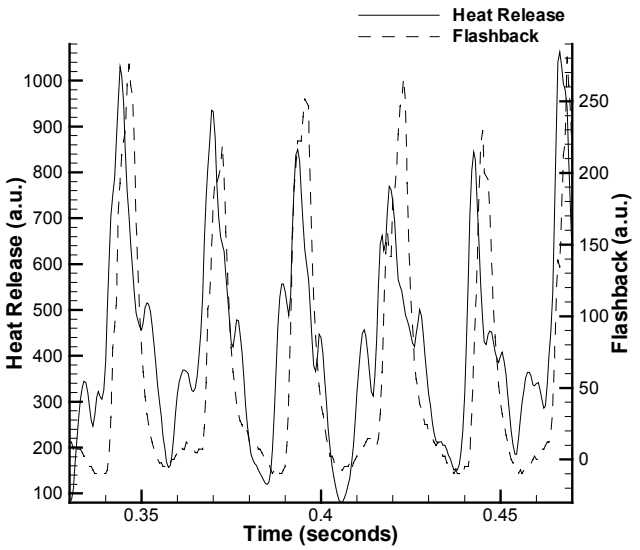

Figure 15. Time History of Flashback and Heat Release Signals (Case 4).

flashback. In the figure one can see the cyclic behavior of heat release due to combustor acoustics. Occasionally spikes are observed in the flashback signal. Note that the flashback signal always lags the heat release signal in time.

Figure 16 shows the power spectral densities of both heat release and flashback signals on a logarithmic (dB) scale. Peak heat release in this case occurs at 40 Hz. and the corresponding flashback photodiode signal has a peak at the same frequency. This implies that flame reaches the location of the fiber optic cable once in every heat release cycle. This effect can also be seen in the time history plot (see Figure 15). Strongest temporal coherence between heat release and flashback signals is also observed at 40 Hz., which corresponds to the peak heat release frequency. Note that in Figure 15 flashback signal peak lags the heat release signal peak by about 3 milliseconds. This time lag is associated with a convective delay of the flame tip flashing back from the dump plane down to the location of the fiber-optic cable.

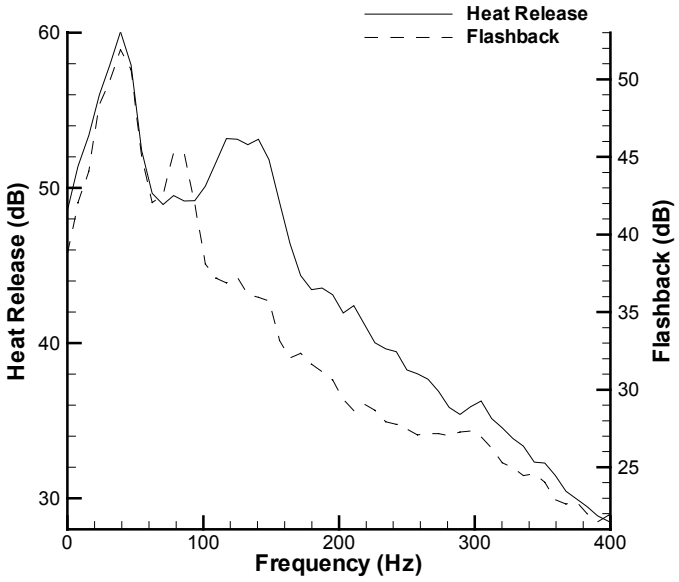

Figure 16. Power Spectra of Heat Release and Flashback Signals (Case 4).

D. Chemiluminescence Measurements

In order to spatially resolve the temporal heat release characteristics inside the main reaction zone and also to track the flame initiation front movement, chemiluminescence measurements of the CH radical were performed. The CH radicals have been shown to be representative of the flame front and CH intensity correlates well with the local heat release. An intensified Princeton Instruments PI-Max 512 T-18 G/III CCD camera with a 512x512 pixel resolution was utilized to acquire the images. The gate duration for the image acquisition was set to 0.10 μs.

A filter mounted on the camera lens is used to transmit the light at λ=430 nm which corresponds to the $B^2\Sigma^-X^2\Pi(0,0)$ emission band of the CH radical[23] and to attenuate all other wavelength contributions. A KISTLER 7061B piezoelectric pressure transducer mounted on the combustor wall provided the phase information. Signal from the pressure transducer is fed into a DSPACE data acquisition board and the trigger signal (a TTL pulse) is generated at the selected phase angle to trigger the camera. To resolve the complete cycle at each phase angle a known time delay is added to the pressure signal. At each

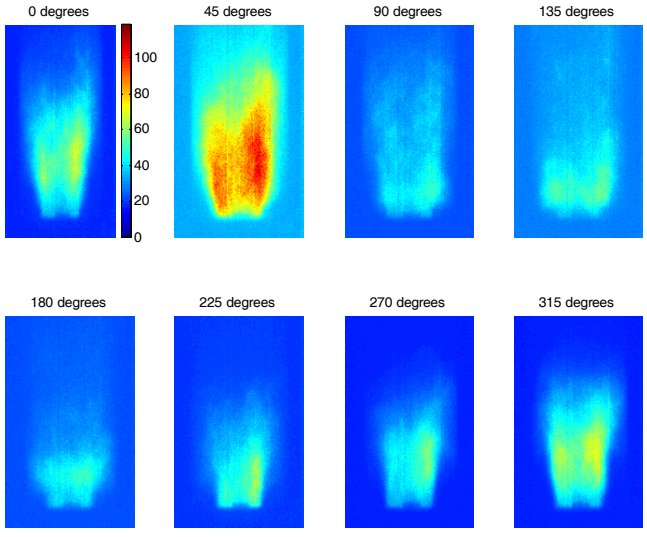

Figure 17. Phase Locked CH Radical Images (Case 5).

triggering condition a sequence of 50 images were recorded. These sequences are then averaged to yield the corresponding mean intensity field.

Figure 17 shows phase locked CH images with 45-degree phase intervals on a pseudo color axis ranging from blue to red. Conical flame initiation front can easily be distinguished from these CH intensity images, as this radical is an excellent marker for a methane flame front. Also CH radical concentration positively correlates with heat release. This particular floe condition at which these images are recorded demonstrates flashback instability. Flame is conical and attached at 0-degree phase angle with respect to acoustic pressure fluctuations. At the next frame (45-degrees) peak heat release is observed, which is evidenced by the large red zone right downstream of the flame initiation front (the interface between blue and green colors). After peak heat release flame de-attaches from the center body (injector) tip and starts propagating upstream. At 180-degree phase instant combustion almost entirely takes place inside the pre-mixing zone as seen in the corresponding frame on the lower left corner.

E. Emission Measurements

Nitric oxide (NO) emission levels were measured and documented for a number of experimental test conditions. Nitric oxide emissions were measured using a chemiluminescence analyzer (Cambustion FNOX400). A custom made water-cooled suction probe sampled the gas at the combustor exhaust.

During the experimental study it is observed that keeping the other variables (equivalence ratio, volumetric flow rate) constant and increasing the hydrogen volume fraction of the fuel results in increased nitric oxide emissions index values. This effect is consistent with the similar observations made in the literature[24]. On the other hand hydrogen enrichment enables combustion at much leaner equivalence ratios[25] than that are ever possible with methane. Premixed lean combustion has long been appreciated as an industry standard technique to reduce nitric oxide emissions. Even though hydrogen addition increases NO_x emissions at a fixed equivalence ratio (see Figure 19) the overall emissions still can be greatly reduced by burning leaner mixtures of methane and hydrogen blend, which were impossible for the pure methane case. This will reduce the adiabatic flame temperature further down reducing the thermal and other contribution to the total NO_x emissions index.

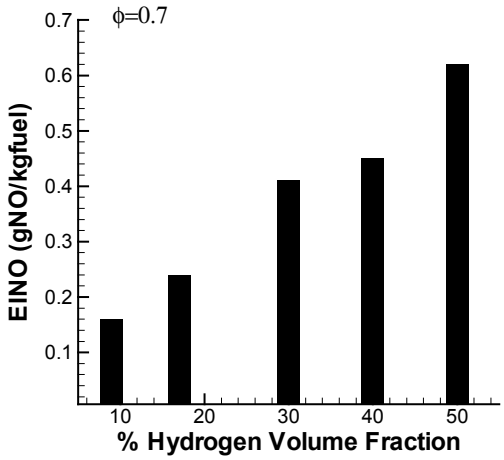

Figure 18. Effect of Hydrogen Enrichment on Emissions Index (Q_{air}=253 lt/min).

F. Flashback Simulations

In this section simulation results of coupled acoustic and hydrodynamic equations are presented in detail. A total of 77 uniformly spaced grid points are used in the radial direction in order to resolve the shape of the flame front. A sufficiently small time step, which enables to capture acoustic oscillations, is used to integrate the model equations. Time integration is stopped in each case only after a stable limit cycle is reached. Due to the non-linearity (saturation effect) in the heat release equation a limit cycle oscillation is quickly established starting from an arbitrary initial condition (see Figure 19). Furthermore, amplitude of this limit cycle depends on the combustor operating conditions. Frequency of this limit cycle is governed by the dominant acoustic mode of the combustor. Peaks observed around 140 Hz. in Figure 20 correspond to this dominant mode for that particular operating condition that they correspond to. As mentioned earlier a single acoustic mode is assumed to be present within the combustor as it can be seen from the Fourier spectra. Mode shape $\psi(x)$ of the standing pressure wave given by Eq. 12 is plotted in Figure 21. The small peak at the third harmonic of the dominant mode (420 Hz.) seen in the heat release spectra is a direct result of the non-linearity in the heat release equation. However, energy contained in this harmonic is much smaller in comparison to the dominant mode. Modes corresponding to higher natural frequencies (in the order of kHz) do not get excited due to the first order filter nature of the heat release equation.

Figure 22 demonstrates the phase locked (with respect to pressure) position of the flame initiation front obtained from numerical simulations. Position of the flame front is shown at 90-degree phase intervals. For this case the ratio of laminar flame speed and mean axial flow velocity u / S_L is 0.6. In a typical pre-mixed gas turbine combustor flame speed Mach number is typically one order of magnitude less than the Mach number of the oncoming fluid flow, similar to the case investigated here. Position of the flame front is determined by solving Eq. 20 numerically. Owing to high frequency fluctuations flame front does not experience excessive curvature, consistent with Dowling's observations. Recall that Figure 17 showed the phase locked position flame front experimentally. In this regard there is a correspondence between these two figures. It is seen from the figure that almost all the time flame is inside the pre-mixing section moving up and down as in the case of experiments. Only around 270-degree phase instant flame attaches the tip of the center-body (injector) briefly and de-attaches again. During this limit cycle

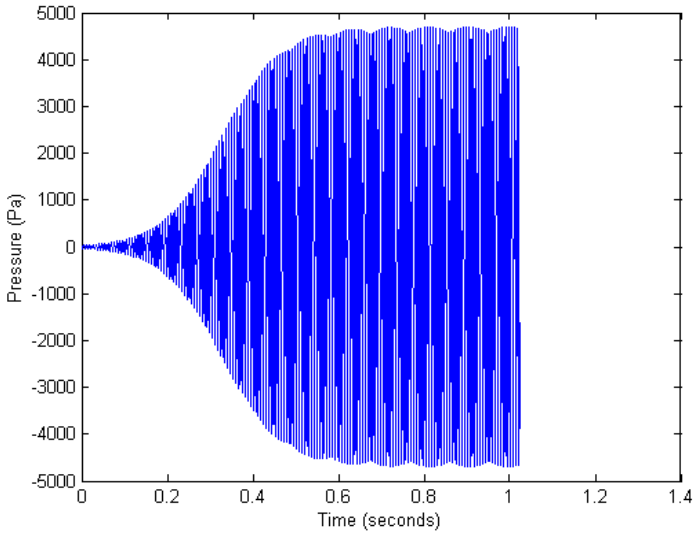

Figure 19. Development of Limit Cycle Pressure Oscillations from an Arbitrary Initial Condition (ϕ=1.0, Q=540 lt/min at x/L=0.85)

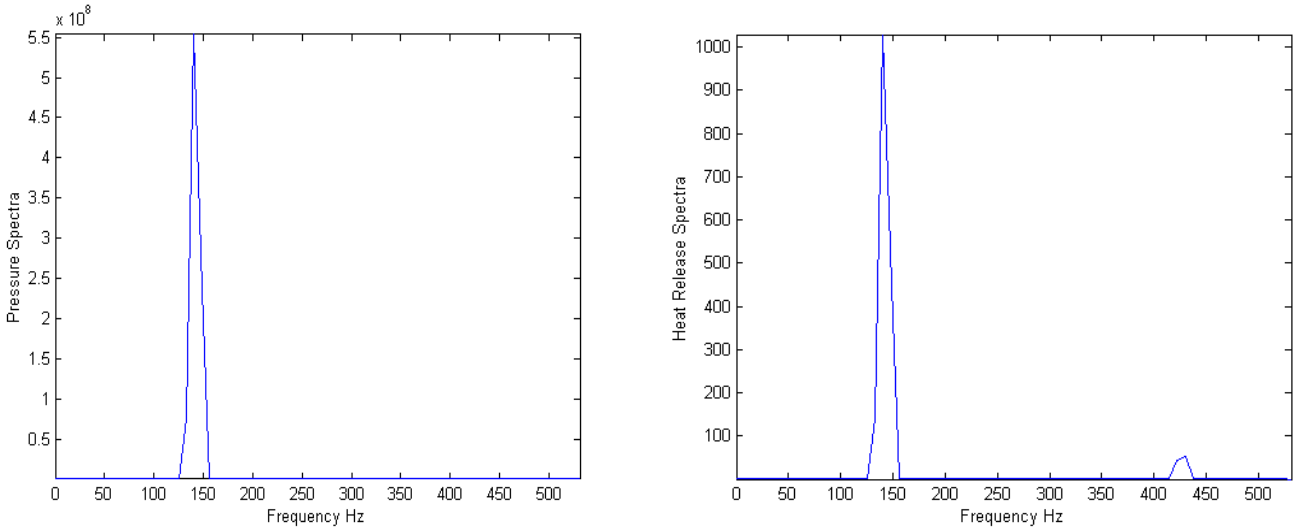

a. Pressure **b. Heat Release**

Figure 20. Pressure and Heat Release Spectra Corresponding to Figure 19.

oscillation flame reaches its maximum propagation distance around 90-degree phase instant at which heat release is at its peak point.

Figure 24 shows the phase plot of flame tip position with respect to limit cycle pressure oscillations corresponding to previous figure. Shape of this curve in the phase plane reminds that of an ellipse. At z=0 the flame is attached at the tip and negative values signify that flame has moved towards the inlet section. Flame propagates up to a non-dimensional distance of z/R=-0.35 which is rather significant, at an instant where peak pressure is reached. This distance on the other hand is rather dependent on the operating condition. This shall be demonstrated in the latter figures. On the contrary flame tip is closer to the dump plane when dynamic pressure is at its minimum.

As in the actual combustor the amplitude of limit cycle oscillations from the simulations depend heavily on the operating conditions. As shown both experimentally and numerically, flashback is directly linked with the amplitude

of these thermo-acoustic limit cycle oscillations. The more intense the pressure fluctuations are, the more upstream distance the flame tip travels during the flashback instability cycle. A change in operating conditions does not affect the combustor acoustics represented by the transfer function $\eta(s)/q(s)$ significantly. However the filter coefficients α and β appearing in Eq. 16 are quite sensitive to the changes in the operating condition. Particularly the gain β of this transfer function has a determining effect on the amplitude of these oscillations. This is because β controls the amount of unsteady heat release input into the acoustic oscillator equation (Eq. 10) is receiving.

Figure 23 shows the RMS amplitude of limit pressure fluctuations obtained from the simulations. RMS pressure amplitude is plotted versus the inlet volumetric flow rate and equivalence ratio. Figures are shown for pressure recorded at x/H=0.85. Recall that locations upstream will experience more intense fluctuations due to the pressure mode shape (see Figure 23) of the pressure wave. The qualitative trends observed Figure match with the trends observed in the actual laboratory combustor. First of all, as the volumetric flow rate is increased RMS pressure amplitude increases substantially. This observation is consistent with the experiments. As there is more fuel is burned at higher flow rates there is more unsteady heat release and this yields in higher RMS fluctuations. In mathematical terms at these flow conditions the term the right hand side of Eq. 10 is larger which gives rise to higher heat release. RMS pressure amplitude is less sensitive to changes in the equivalence ratio in comparison to flow rate. Nevertheless, there is a slight increase in pressure fluctuation amplitude with increasing equivalence ratio. This increase can be attributed to the increase in the filter gain β appearing in Eq. 10. Note that this parameter is closely related with the forward reaction rate and the forward reaction rate increases as the equivalence ratio increases until it reaches stoichiometric condition where the reaction proceeds fastest.

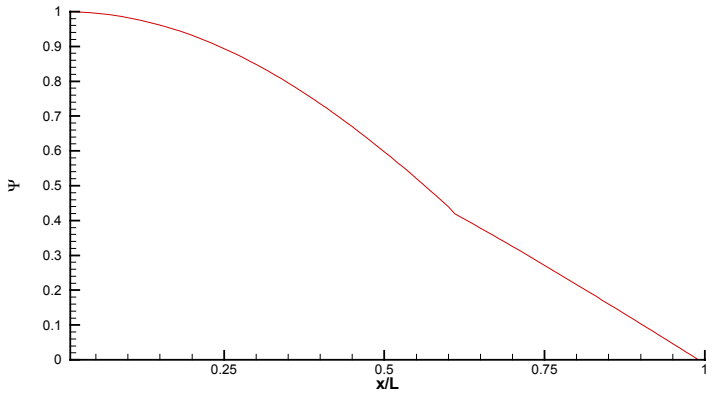

Figure 21. Mode Shape of Acoustic Pressure Corresponding to Figure 19.

Last figure (see Figure 25) shows the maximum flame propagation distance, measured from the combustor dump plane, during the instability cycle. One can spot the close correspondence of this figure (Figure 25) with the previous one (Figure 23). The more intense the pressure fluctuations are the more upstream flame propagates during the instability cycle. Of course flashback is facilitated by higher flame speeds, however it is observed that acoustic velocities are typically an order of magnitude larger than laminar flame speeds. Therefore, flashback is mostly related with pressure perturbations. Flame speed, which is proportional with the reaction rate, manifests itself in the filter gain β appearing in Eq. 10. This is the reason why, at larger flame speeds (larger β thus more intense fluctuations) flashback activity

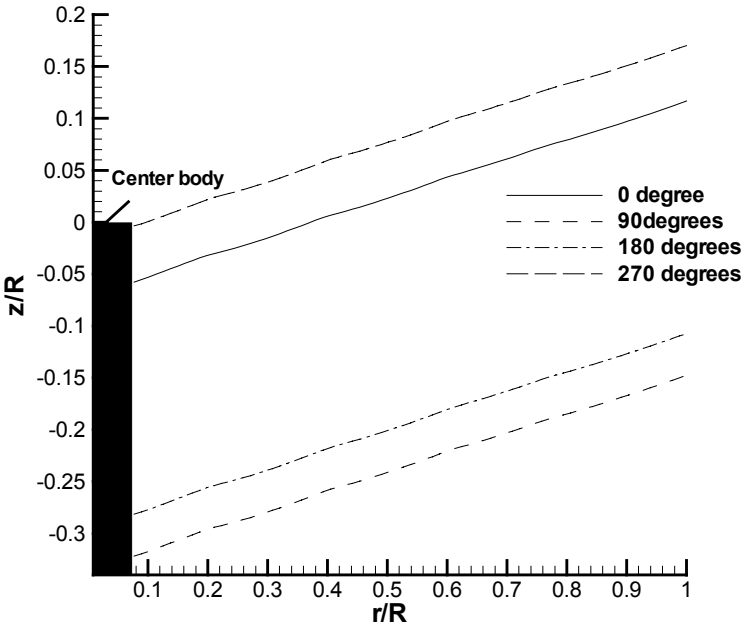

Figure 22. Flame Front Movement with Respect to Thermo-acoustic Instability Cycle Corresponding to Figure 19.

is more intense.

V. Conclusion

A mathematical model has been developed in order to identify the thermo-acoustic instability induced flame flashback and flame holding characteristics. In addition, experiments were conducted using pure and hydrogen enriched methane of varying composition as the fuel gas. Generally good qualitative agreement is observed between theory and experiments.

First of all, thermo-acoustic instability induced flashback could be realistically simulated using the developed mathematical model. Due to the non-linear nature of the coupling between heat release and mass flow perturbations a stable limit cycle whose amplitude is dependent on flow conditions is observed. Introduced non-linearity is of ad-hoc nature, which has a certain physical justification to it as explained earlier. Nevertheless, one can conclude post-hoc that the results closely mimic the actual combustor behavior (limit cycle, flashback, RMS pressure etc.). Furthermore, this paper clearly identifies thermo-acoustic instability as a driving cause of flashback instability.

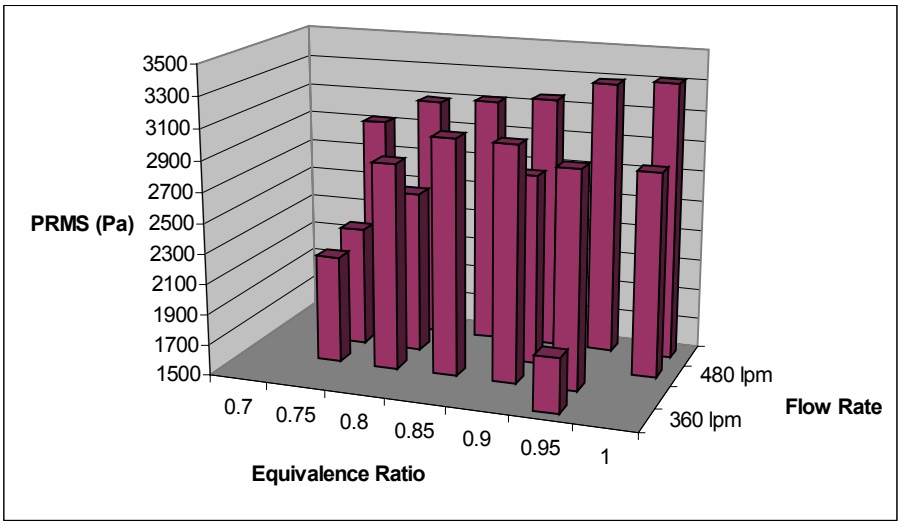

Figure 23. RMS Amplitude of Limit Cycle Pressure Oscillations at x/L=0.85.

Hydrogen addition to methane substantially extends lean flammability limits. Lean combustion enables very low nitric oxide emission levels (typically only a few ppm) to be achieved. This is the main benefit of hydrogen enrichment. Otherwise adding hydrogen to the mixture and keeping all the other variables fixed increases nitric oxide levels. This effect is due to the existence of a richer OH radical pool, which boosts nitric oxide formation rates, due to hydrogen enrichment. Using the present definition of equivalence ratio, adiabatic flame temperature does not change with increasing hydrogen content at a fixed equivalence ratio. Combustion takes place sequentially, hydrogen is consumed under stochiometric conditions then the leftover oxygen oxidizes methane. Therefore, one can rule out the effect of temperature change, as a possible cause of increased NO emissions.

In order to prevent the occurrence of flashback attention should be focused primarily on killing the low frequency pressure fluctuations. If the instability occurs at a rather low frequency then the period of oscillations are larger which

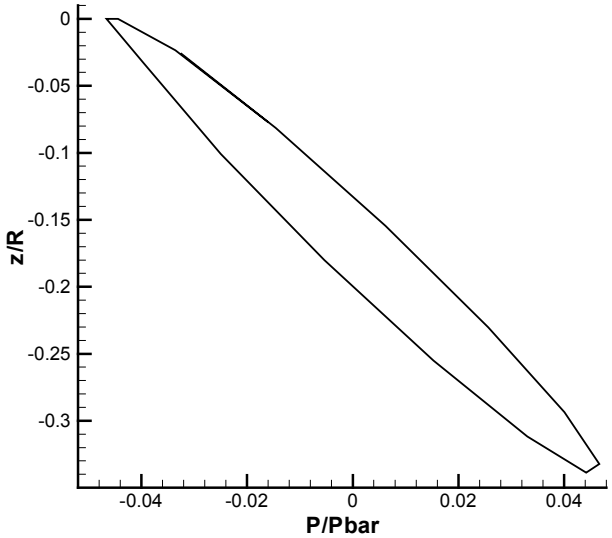

Figure 24. Phase Plot of Flame Tip Location with Respect to Pressure Oscillations Corresponding to Figure 19.

gives the flame plenty of time to propagate upstream when flow reversal occurs.

Part of the future work is aimed at developing active control strategies in order to stabilize the flame front movement. It is observed that flashback is primarily triggered by thermo-acoustic instability. Acoustic velocities are typically an order of magnitude larger than laminar flame speeds. Therefore, an active control scheme designed to suppress the amplitude of thermo-acoustic limit cycle oscillations is also anticipated to help resolve the flashback issue. Numerical details about resolving the flame hydrodynamics shall be discussed in great detail in a prospective paper along with a parametric study covering a variety of load conditions. Another research prospect is to couple this model with a multi-step reduced chemical kinetics scheme for $H_2/CO/CH_4$ (methane + synthesis gas) mixtures and study the effect of acoustics, flame hydrodynamics and mixture composition on nitric oxide and carbon monoxide emissions. Present paper assumes a one step global chemistry to determine reaction rate and linearizes it to obtain heat release filter coefficients. However, a more detailed reaction mechanism without any linearization would enable a better understanding of these aforementioned phenomena within a single more complete mathematical framework.

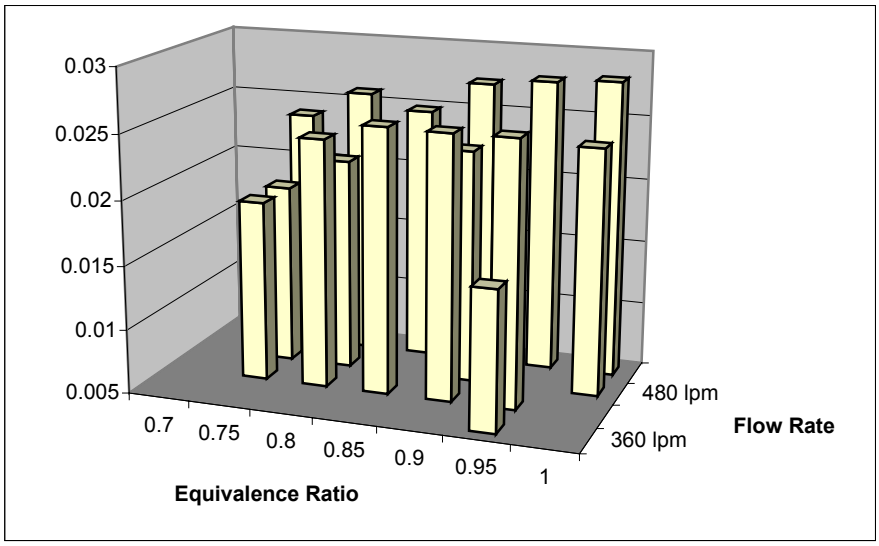

Figure 25. Maximum Distance Traveled Upstream by the Flame Tip During One Cycle (m).

Appendix

Taking the gradient along the radial direction $\partial/\partial r$ of both sides in order to transform the dynamic flame front equation (Eq. 20) into a weakly hyperbolic conservation equation form one arrives at the following expression,

$$\frac{-\partial^2 f}{\partial r \partial t} + \frac{\partial u}{\partial r} = S_L \frac{\partial}{\partial r}\left(\sqrt{1+\left(\frac{\partial f}{\partial r}\right)^2}\right) \tag{A.1}$$

Re-arranging the above such that,

$$\frac{\partial^2 f}{\partial r \partial t} + S_L \frac{\partial}{\partial r}\left(\sqrt{1+\left(\frac{\partial f}{\partial r}\right)^2}\right) = \frac{\partial u}{\partial f}\frac{\partial f}{\partial r} \tag{A.2}$$

Defining a new variable as the gradient of the flame front in the radial direction,

$$\xi = \frac{\partial f}{\partial r} \tag{A.3}$$

Eq. 20 simplifies into a conservation equation form such that the time derivative of ξ plus a flux term equals to the source term.

$$\frac{\partial \xi}{\partial t} + S_L \frac{\partial}{\partial r}\left(\sqrt{1+\xi^2}\right) = \frac{\partial u}{\partial f}\xi \tag{A.4}$$

Now this equation is discretized in space using a 5th order WENO scheme and integrated in time using a 3rd order accurate total variation diminishing Runge-Kutta scheme. Further details on discretization and time details are not presented in this text. However, since one is only solving for ξ which is the derivative of the single valued flame

front function in the radial direction, it is necessary to re-construct f in every time step. This is simply achieved by integrating ξ along the radius starting at the center body r=a.

$$f(r,t) = \int_a^r \xi(r,t)dr + f(a,t) \tag{A.5}$$

In the above equation the term $f(a,t)$ represents the position of the flame tip in time. While taking the gradient of Eq. 20, this information is lost. Therefore, it is necessary to track the tip of the flame in time separately.

$$\left.\frac{\partial f}{\partial r}\right|_{r=a} = \begin{cases} \dfrac{\left(u^2 - {S_L}^2\right)^{1/2}}{S_L} & if \quad u(t) \geq S_L \wedge \quad f(a,t) = 0 \\ 0 \quad if \quad u \leq S_L \vee \quad f(a,t) < 0 \end{cases} \tag{A.6}$$

By integrating the above expression in time the information flame tip is recovered. It is assumed that at t=0 the flame is attached at the tip.

$$f(a,t) = \int_0^t \frac{\partial f}{\partial t} dt \tag{A.7}$$

Acknowledgments

This work would not be possible without the financial support obtained from CPERC (Clean Power and Energy Research Consortium). Authors would like to express their sincere gratitude for this support. The help and support received from Mr. Jeffrey Wilbanks in the various facets of the work is gratefully acknowledged as well.

References

[1]Lawn, C. J., "Interaction of the Acoustic Properties of a Combustion Chamber with Those of Premixture Supply", *Journal of Sound and Vibration*, Vol. 224, 1999, pp. 785-808.

[2]Westbrook, C. K., and Dryer, F. L., "Chemical Kinetic Modeling of Hydrocarbon Combustion", *Prog. Energy Combustion Science*, Vol. 10, 1984, pp. 1-57.

[3]Zimont, V. L., "The Theory of Turbulent Combustion at High Reynolds Numbers", *Combustion Explosions and Shock Waves*, Vol. 15, 1979, pp. 305-311.

[4]Dowling, A. P., "The Calculation of Thermoacoustic Oscillations", *Journal of Sound and Vibration*, Vol. 180, 1995, pp. 557-581.

[5]Kiesewetter, F., Hirsch, C., Fritz, M., Kroner, M. and Sattelmayer, T., "Two-Dimensional Flashback Simulation in Strongly Swirling Flows", *International Gas Turbine and Aeroengine Congress and Exposition*, ASME 2003-GT-38395, Atlanta, Georgia, USA, 2003.

[6]Lord Rayleigh, "The Theory of Sound", London, Macmillian, 1896.

[7]Tuncer, O., Acharya, S., Banaszuk, A. and Cohen, J., "Side Air Jet Modulation for Control of Heat Release and Pattern Factor", *International Gas Turbine and Aeroengine Congress and Exposition*, ASME 2003-GT-38853, Atlanta, Georgia, USA, 2003.

[8]Umurhan, O. M., "Exploration of Fundamental Matters of Acoustic Instabilities in Combustion Chambers", *Center for Turbulence Research Annual Briefs*, 1999, pp. 85-98.

[9]Smoot, L. D. and Smith, P.J., "Coal Combustion and Gasification", Plenum Press, New York, 1985.

[10]Tomzcak, H., Benelli, G., Carrai, L. and Cecchini, D., "Investigation of a Gas turbine Combustion System Fired with Mixtures of Natural Gas and Hydrogen*", IFRF Combustion Journal*, Article Number: 200207, 2002.

[11]Cowell, L. Etheridge, C. and Smith, K., "Ten Years of Industrial Gas Turbine Operating Experiences", *International Gas Turbine and Aeroengine Congress and Exposition,* ASME 2002-GT-30280, Amsterdam, The Netherlands, 2002.

[12]Mariotti, M., Tanzini, G., Faleni, M. and Castellano, L., "Sperimentazione di Fiamme di Idrogeno a Pressione Atmosferica in un Combustore per Turbogas con Iniezione di Inerti", Technical report, Enel Produzione, Pisa, Italy, ENELP/RIC/RT/-2002/0063, 2002.

[13]Calvetti, S., Carrai, L. and Cecchini, D., "Esecuzione di Prove di Co-Combustione di Gas Naturale e Syngas da Biomassa su un Combustore DLN per Turbina-Gas", Technical report, Enel Produzione, Pisa, Italy, ENELP/RIC/RT/-2001/258/0-IT+RT.RIC.PI, 2001.

[14]Calvetti, S., Carrai, L. and Cecchini, D., "Progettazione di un Combustore DLN Prototipo per TG per la Co-Combustione di Gas Naturale e Syngas da Biomassa", Technical report, Enel Produzione, Pisa, Italy, ENELP/RIC/RT/-2001/146/0-IT+RT.RIC.PI, 2001.

[15]Lee, D. H. and Lieuwen, T., "Premixed Flame Kinematics in a Longitudinal Acoustic Field", *Journal of Propulsion and Power*, Vol. 19, 2003, pp. 837-846.
[16]Eisenhower, B. A., "Identification of Thermoacoustic Dynamics Exhibiting Limit Cycle Behavior", Master's Thesis, Virginia Polytechnic Institute and State University, Blacksburg, VA, 2000.
[17]Park, S., Annaswamy, A. and Ghoneim, A., "Heat Release Dynamics Modeling of Kinetically Controlled Burning", *Combustion and Flame*, Vol. 128, 2002, pp. 217-231.
[18]Markstein, G. H., "Non-Steady Combustion Propagation", The Macmillan Company, Pergamon Press, Oxford, 1964.
[19]Dowling, A. P., "A Kinematic Model of a Ducted Flame", *Journal of Fluid Mechanics*, Vol. 394, 1999, pp. 51-72.
[20]Jones, B., "Reheat Buzz Film", Combustion Department, Rolls-Royce Derby, 1974.
[21]Beer, J. M. and Chigier, N. A., "Combustion Aerodynamics", Applied Science Publishers, London, 1972.
[22]Yu. G., Law, C. K. and Wu, C. K., "Laminar Flame Speeds of Hydrocarbon Plus Air Mixtures with Hydrogen Addition", *Combustion and Flame*, Vol. 63, 1986, pp. 339-347.
[23]Garland, N. L. and Crosley, D.R., "Energy Transfer Processes in CH $A^2\Delta$ and $B^2\Sigma^-$ in an Atmospheric Pressure Flame", *Applied Optics*, Vol. 24, 1985, pp. 4229-4237.
[24]Schefer, R. W.,"Reduced Turbine Emissions Using Hydrogen Enriched Fuels", *Proceedings of the 2002 U.S. DOE Hydrogen Program Review*, NREL/CP-610-32405, 2002.
[25]Bell, S. R. and Gupta, M., "Extension of the Lean Operating Limit for Natural Gas Fueling of a Spark Ignited Engine Using Hydrogen Blending", *Combustion Science and Technology*, Vol. 123, 1997, pp. 23-47.